

We are IntechOpen, the world's leading publisher of Open Access books Built by scientists, for scientists

6,900

Open access books available

186,000

International authors and editors

200M

Downloads

Our authors are among the

154

Countries delivered to

TOP 1%

most cited scientists

12.2%

Contributors from top 500 universities



WEB OF SCIENCE™

Selection of our books indexed in the Book Citation Index
in Web of Science™ Core Collection (BKCI)

Interested in publishing with us?
Contact book.department@intechopen.com

Numbers displayed above are based on latest data collected.
For more information visit www.intechopen.com



Planar Antenna Array Hybrid Beamforming for SDMA in Millimeter Wave WPAN

Sau-Hsuan Wu, Lin-Kai Chiu, Ko-Yen Lin and Ming-Chen Chiang
*Institute of Communication Engineering
Department of Electrical Engineering
National Chiao Tung University
Hsinchu, Taiwan*

1. Introduction

The increasing demands on bandwidth for personal and indoor wireless multimedia applications have driven the research and development for a new generation of broadband wireless personal area network (WPAN) Alliance (n.d.); *IEEE 802.11 WLAN Very High Throughput in 60GHz* (n.d.); *IEEE 802.15 WPAN Millimeter Wave Alternative PHY Task Group (TG3c)* (n.d.); *WirelessHD* (n.d.). This new WPAN is intended to support data rate up to 5Gbps or more and allows for wireless interconnection among devices, such as laptops, camcorders, monitors, DVD players and cable boxes, etc. Moreover, it could also serve as a wireless alternative to the High-Definition Multimedia Interface (HDMI).

In addition to its very large bandwidth, the new WPAN also demands for short-range and secure wireless connections. The characteristics of broad unlicensed bandwidth FCC (2004), high penetration loss Smulders (1995; 2002) and significant oxygen absorption Anderson & Rappaport (2004) at 60GHz radio make it an ideal wireless interface for the next generation WPAN. Furthermore, the millimeter wavelength of 60GHz radio also makes it possible to use tens of tiny antennas to steer radio signals with high directivity to the intended receivers. This feature of high-directivity beam pattern not only improves the wireless link quality Balanis & Ioannides (2007) but also increases the spatial reuse factor, allowing for multiple users to gain access to the wireless channel at the same frequency and time. In view of the great potential of 60GHz radio on WPAN and the advantages of beamforming (BF) for millimeter wave (mmWave) applications, we study in this article a simple hybrid beamforming (HBF) technique for spatial division multiple access (SDMA) using planar antenna arrays (PAAs).

Digital BF has been used to compensate the rather fixed radiation patterns of switch-beam or beam-selection antennas to create more flexible hybrid beam patterns Celik et al. (2006); Rezk et al. (2005); Zhang et al. (2003). In conjunction with the phase shifters of the element antennas of PAAs, a hybrid type of BF is considered in Smolders & Kant (2000) which exploits the advantage of BF both in the baseband and the radio-frequency (RF) ranges. Motivated by the above results and taking into account the practical limitation and implementation cost of the full digital BF, we study herein a special type of baseband and RF HBF for SDMA that only requires four digital processing paths to support HBF on a 8×8 PAA illustrated in Fig. 1. The entire PAA of Fig. 1 is partitioned into four blocks of patch antennas. Each block is driven by a digital BF weight, while each element patch antenna in a block is equipped with

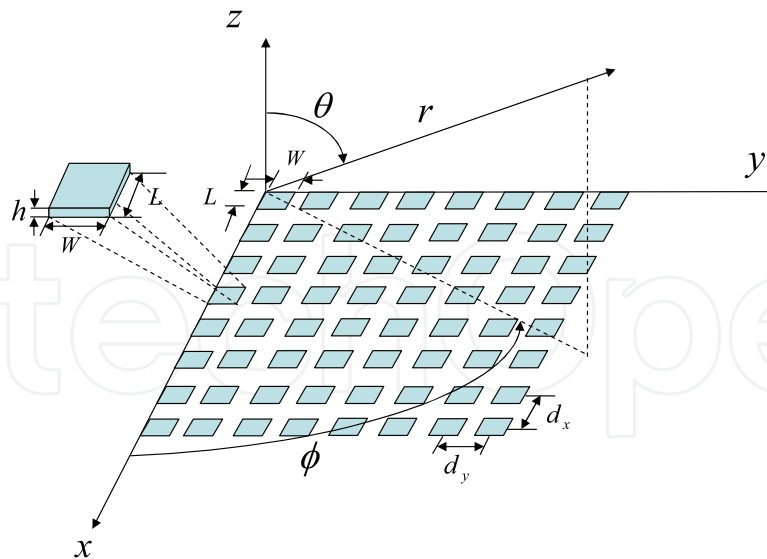


Fig. 1. Antenna arrays of 8×8 planar antennas.

an individual phase shifter. With this configuration, we study the design of HBF for two-user SDMA and compare its performance with that of RF BF only.

The content of this chapter is organized in the following order. First, some concept and the configuration about PAA will be reviewed in Section II and applied to SDMA using reconfigurable PAA. In Section III, the baseband-and-RF hybrid BF (HBF) will be introduced for SDMA, and the linear constrain minimum power (LCMP) digital BF technique will be reapplied to this new setting of PAA HBF over mmWave radio. The signal to interference-plus-noise ratios (SINRs) of users with the aforementioned BF scheme will be investigated in Section IV and the BER simulations will also be conducted on an OFDM-based WPAN to verify the performance of HBF for SDMA over mmWave radio. Conclusions will be drawn in Section V.

2. The configurations of planar antenna arrays

We specify in this section the configurations of planar antenna arrays (PAA) for hybrid BF. Sixty-four identical patch antennas are aligned to form an 8×8 antenna matrix as shown in Fig. 1. Each element antenna is equipped with a phase shifter to maneuver the phase of the signal radiating through it. Given the large number of antennas available for 60GHz applications, it is beneficial to use the antennas to serve multiple users in addition to increasing the received signal to noise ratio (SNR) of a single user. Taking into account the practical limitations of circuit implementations, the arrays of antennas are partitioned into blocks, and each of which is driven by a baseband signal processing path. In other words, the baseband BF weights are applied to the antennas on a block basis. Antennas within the same block are applied the same baseband BF weight. In this section, we characterize the beam pattern of this hybrid type of radio-frequency (RF) and baseband (BB) BF.

To facilitate the analysis and highlight the performance of hybrid BF (HBF), the coupling effects among element antennas are neglected in the sequel. As a result, the total beam pattern of a block of a partition can be expressed as the product of the electric field of a single antenna and the array factor corresponding to the block Balanis (1997).

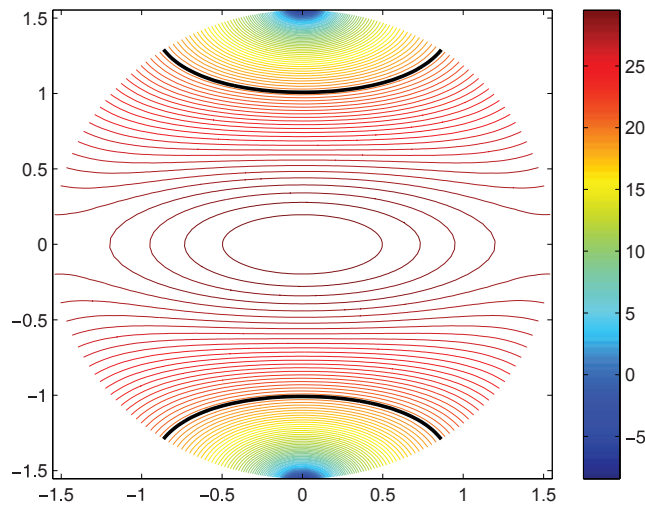


Fig. 2. The contour plot of the antenna pattern when $P=30$ dB.

The far-zone electric field of a single element antenna is given by

$$E(\phi, \theta) = E_\theta \vec{a}_\theta + E_\phi \vec{a}_\phi + E_r \vec{a}_r \quad (1)$$

where

$$E_\theta = j \frac{hWkE_0 e^{-jkr}}{\pi r} \left[\cos \phi \cos X \left(\frac{\sin Y}{Y} \right) \left(\frac{\sin Z}{Z} \right) \right] \quad (2)$$

$$E_\phi = j \frac{hWkE_0 e^{-jkr}}{\pi r} \left[\cos \theta \sin \phi \cos X \left(\frac{\sin Y}{Y} \right) \left(\frac{\sin Z}{Z} \right) \right] \quad (3)$$

and $E_r \cong 0$ as $r \gg \frac{2LW}{\lambda}$ (see Balanis (1997) for the far field definition). The physical meaning of some of the parameters are illustrated in Fig. 1, and E_0 is a constant. For convenience of expression, we also define $X \triangleq \frac{kL}{2} \sin \theta \cos \phi$, $Y \triangleq \frac{kW}{2} \sin \theta \sin \phi$, $Z \triangleq \frac{kh}{2} \cos \theta$ and $k \triangleq \frac{2\pi}{\lambda}$ with λ being the radio wavelength.

The contour plot of the electric field is shown in Fig. 2 as $P|E(\phi, \theta)|^2$ in dB in the cylindrical coordinate, with $P = 30$ dB. The dimensions of the element patch antenna used in the simulation are $L = W = 1$ mm, $h = 0.1$ mm and the distances between adjacent antennas are set to $dx = dy = 2.5$ mm. The radial coordinate is mapped to the elevation angle θ and the angular coordinate is to the azimuth angle ϕ of the antenna pattern. The vertical coordinate displays the antenna gain in decibel. We note that the antenna pattern is not symmetric with respect to the azimuth angle, ϕ . The pattern is narrower in the direction of $\phi \pm \pi/2$.

The array factor of each block depends on its relative position in the PAA. For the partition shown in Fig. 3, we define an index pair, $(p, q) \in \{0, 1\}^2$, for each block of the PAA. Given the index pair (p, q) of a block, the corresponding array factor follows

$$A_{(p,q)}(\phi, \theta) = e^{jpN(\Psi_x + \beta_{x,(p,q)})} \sum_{n=1}^N e^{j(n-1)(\Psi_x + (-1)^p \beta_{x,(p,q)})} \times e^{jqM(\Psi_y + \beta_{y,(p,q)})} \sum_{m=1}^M e^{j(m-1)(\Psi_y + (-1)^q \beta_{y,(p,q)})} \quad (4)$$

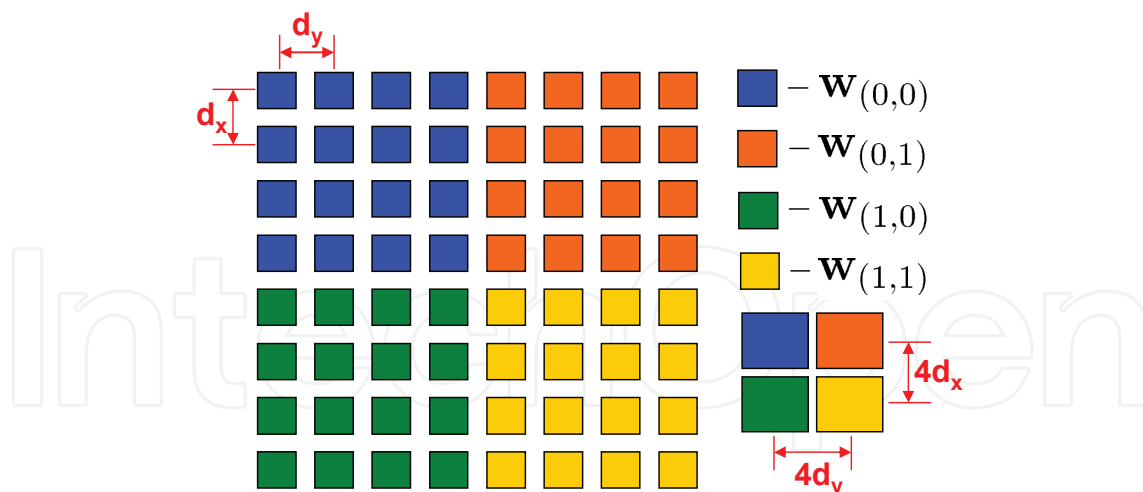


Fig. 3. Partitions of the planar antenna arrays. Patch antennas in different color belong to different block.

where $\Psi_x \triangleq kd_x \cos \phi \sin \theta$ and $\Psi_y \triangleq kd_y \sin \phi \sin \theta$. The distances in the x and y directions between adjacent patch antennas are denoted by d_x and d_y , respectively. And $\beta_{x,(p,q)}$ and $\beta_{y,(p,q)}$ are the corresponding phase differences in the x and y directions between adjacent patch antennas. The number of antennas in the x direction of a block is M and the number of antennas in the y direction is N . Given the desired direction $(\phi_{d,(p,q)}, \theta_{d,(p,q)})$ set for the block (p, q) , $\beta_{x,(p,q)}$ and $\beta_{y,(p,q)}$ are equal to

$$\beta_{x,(p,q)} = (-1)^{p+1} kd_x \sin \theta_{d,(p,q)} \cos \phi_{d,(p,q)} \pm 2c_1 \pi \quad (5)$$

$$\beta_{y,(p,q)} = (-1)^{q+1} kd_y \sin \theta_{d,(p,q)} \sin \phi_{d,(p,q)} \pm 2c_2 \pi \quad (6)$$

where c_1 and c_2 are any integers. It is noted that the array factor (4) is a periodic function with a period of 2π and is zero whenever (ϕ, θ) satisfy either one of the following two conditions

$$\Psi_x + (-1)^p \beta_{x,(p,q)} = 2c_3 \pi / N \quad (7)$$

$$\Psi_y + (-1)^q \beta_{y,(p,q)} = 2c_4 \pi / M \quad (8)$$

when c_3 and c_4 are integers not equal to the multiples of N and M , respectively.

2.1 SDMA using reconfigurable PAA

Adjusting the antenna phases of a block based on (4) ~ (8), the main beams of different blocks can be tuned towards the directions of different users, offering spatial division to support multiple access (SDMA) of users. Despite the array gain provided by (4), the SINR of SDMA also depends on the antenna pattern of (1) and the beam patterns of adjacent users.

Suppose that all patch antennas in Fig. 3 are used to support a single user. The maximum achievable array gain in this case is $20 \log_{10}(64) \doteq 36$ dB when

$$\Psi_x + (-1)^p \beta_{x,(p,q)} = 2c_5 \pi \quad (9)$$

$$\Psi_y + (-1)^q \beta_{y,(p,q)} = 2c_6 \pi, \{c_5, c_6\} \in \mathbb{Z} \quad (10)$$

where \mathbb{Z} stands for the integer number. Fig. 4 shows the contour plot of the corresponding array pattern when $\theta_{d,(0,0)} = 0$. It is clear that the maximum array gain of 36 dB is achieved

at $\theta = \theta_{d,(0,0)} = 0$. Scaling the power by $1/MN$ for each element antenna of the $M \times N$ PAA, the maximum effective array gain is $10 \log_{10}(64) \doteq 18$ dB.

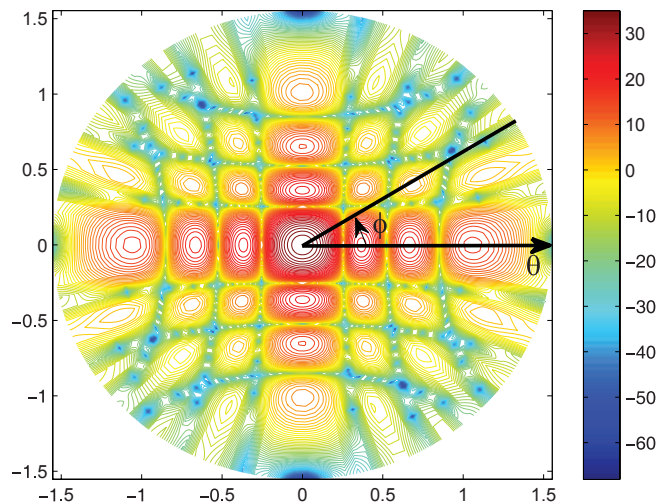


Fig. 4. Contour plot of the array pattern for one-user case when $\theta_{d,(0,0)} = 0$.

On the other hand, if each block in Fig. 3 serves a user with an 4×4 antenna array, the maximal array gain now reduces to a smaller value of $20 \log_{10}(16) \doteq 24$ dB. Except for the smaller array gain, each user's signal is also interfered by the signals of adjacent users. Fig. 5 shows the array factors for the 4-user SDMA based on the partition in Fig. 3. The four beams are pointed toward the elevation angle of $\frac{\pi}{4}$ and the azimuth angles of $\frac{i\pi}{4}$, $i = 1, \dots, 4$, respectively. As can be seen from the figures, the side beams of adjacent users overlap with the main beam of the user of interest, making it difficult to maintain the SINR in practice. To provide a better control for the SINRs of users supported with PAA, a hybrid approach of BF (HBF) is introduced in the next section to take the advantage of baseband BF techniques.

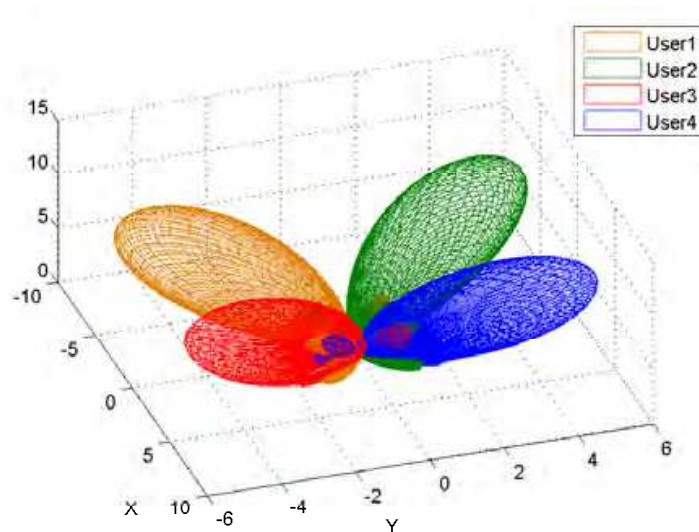


Fig. 5. The array factors of the 4-user SDMA based on the partition in Fig. 3.

3. SDMA using hybrid beamforming

The SDMA method introduced in Section 2.1 is based on phase adjustment with the phase shifter of each element antenna. However, adjusting only the phases of the radio signals sometimes may not be able to achieve the desired SINR for the user of interest, as the beam direction of the user might be severely jammed by the side beams of other users. To overcome this difficulty, baseband BF techniques can be used to jointly steer the beam patterns and suppress the interference for all users. More specifically, in addition to steering the main beam towards the direction of interest, the baseband array factor can be nulled as well in the directions of other users' main beams.

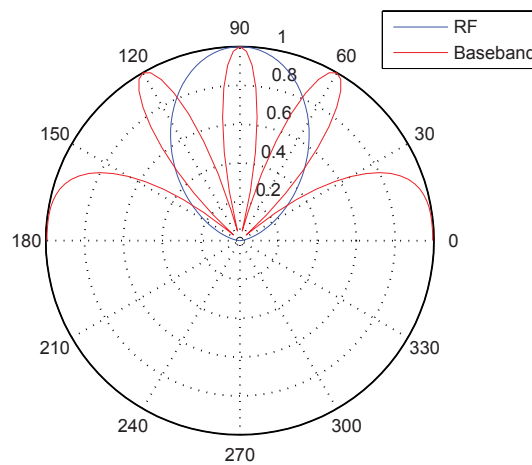


Fig. 6. The polar plot of the HBF pattern with the partition in Fig. 3 when $\theta_d = \pi/2$.

However, it is impractical to apply a baseband BF weight for each element antenna of the 8×8 PAA. Taking into account the implementation cost, each partition of PAA is driven by a common baseband BF weight, while each antenna is still equipped with an individual phase shifter. To distinguish the array factor $B(\phi, \theta)$ formed with the baseband BF weights of a user from the array factor $A(\phi, \theta)$ obtained by tuning the phase of the radiated wave of each antenna, we refer to $B(\phi, \theta)$ as the baseband array factor (BAF) in contrast to the array factor $A(\phi, \theta)$ tuned in the radio-frequency (RF) band.

Now we consider this hybrid type of baseband and RF BF for the simple partition shown in Fig. 3. Suppose that the RF array factor (RAF) for different blocks of a user are the same and pointed to the desired direction of interest, the composite beam pattern of HBF is given by

$$H(\phi, \theta) \triangleq B(\phi, \theta)A(\phi, \theta)E(\phi, \theta) \quad (11)$$

where $A(\phi, \theta)$ is the array factor of the 4×4 antenna arrays. In the extreme case of Fig. 3 that the entire PAA is used to support a single user, the BAF is given by

$$B(\phi, \theta) = \sum_{r=0}^1 \sum_{s=0}^1 w_{(r,s)} e^{j4r\Psi_x} e^{j4s\Psi_y}. \quad (12)$$

where $\Psi_x \triangleq kd_x \cos \phi \sin \theta$ and $\Psi_y \triangleq kd_y \sin \phi \sin \theta$. The enlarged distances between the adjacent effective antennas make $4kd_x = 4kd_y = 4\pi$ in (12) as $dx = dy = \lambda/2$, which in turn

results in the periodic baseband beam pattern of $B(\phi, \theta)$ shown in Fig. 6. The angular coordinate corresponds to the elevation angle θ and the radial coordinate represents the normalized BF gain. Due to the periodic pattern, the product of $B(\phi, \theta)$ and $A(\phi, \theta)$ will yield significant sidelobes on both sides of the main beam. For clarity, the RAF $A(\phi, \theta)$ of the 4×4 block is also shown in Fig. 6. Since the patch antenna has a fixed radiation pattern, its pattern is not shown in the figure.

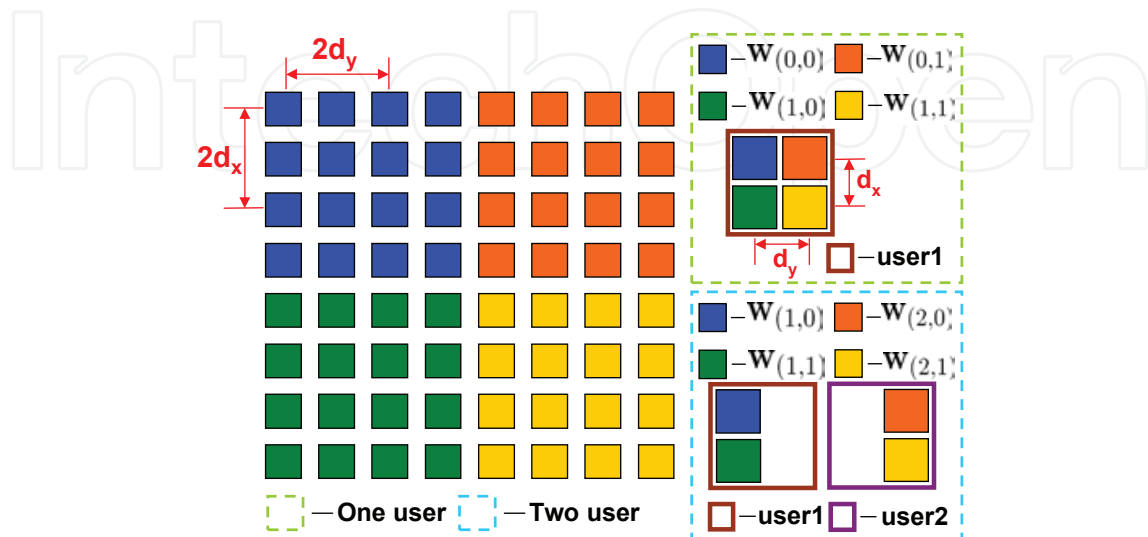


Fig. 7. The partition of the PAA for two-user SDMA, where patch antennas of the same color belong to the same block.

3.1 HBF based on the MD beamforming

According to the configuration of Fig. 3, we now implement HBF for two-user SDMA based on the partition in Fig. 7. The antennas in blue and green colors of Fig. 7 belong to user one, and the antennas in orange and yellow belong to user two. Namely, two BF weights are employed for each user. The resultant BAF for user one and two are given by

$$B_1(\phi, \theta) = w_{(1,0)} + w_{(1,1)}e^{j\Psi_x} \quad (13)$$

$$B_2(\phi, \theta) = w_{(2,0)}e^{j\Psi_y} + w_{(2,1)}e^{j\Psi_x + j\Psi_y}. \quad (14)$$

Now to steer the main beam towards the direction of the user of interest and, in the mean time, to suppress the interference in the direction of the other user, a typical method is the so-called maximum directivity (MD) BF Kuhwald & Boche (1999).

The MD BF basically constructs the baseband BF weights by superposition of the steering vectors

$$\mathbf{s}_1(\phi, \theta) \triangleq [1 \ e^{j\Psi_x}]^T \quad (15)$$

$$\mathbf{s}_2(\phi, \theta) \triangleq [e^{j\Psi_y} \ e^{j(\Psi_x + \Psi_y)}]^T \quad (16)$$

of user one and two in (13) and (14), respectively. Specifically, the BAFs are expressed as

$$B_1(\phi, \theta) \triangleq \sum_{i=1}^2 b_i [1 \ e^{-j\Psi_{xi}}] \mathbf{s}_1. \quad (17)$$

$$B_2(\phi, \theta) \triangleq \sum_{i=1}^2 c_i [e^{-j\Psi_{yi}} \ e^{-j(\Psi_{xi} + \Psi_{yi})}]^H \mathbf{s}_2 \quad (18)$$

where $\Psi_{xi} \triangleq 4kd_x \cos \phi_i \sin \theta_i$ and $\Psi_{yi} \triangleq 4kd_y \sin \phi_i \sin \theta_i$, and $\{\phi_i, \theta_i\}$ is the desired beam direction of user i . Substituting the constraints of

$$B_m(\phi_i, \theta_i) = \begin{cases} 1, & i = m \\ 0, & i \neq m \end{cases}, \quad i, m \in \{1, 2\}. \quad (19)$$

back into (17) and (18) yields the coefficients b_i and c_i . Furthermore, equating the $B_m(\phi, \theta)$ respectively for $m \in \{1, 2\}$ in (13) ~ (18) results in the baseband BF weights

$$w_{(1,r)} = \sum_{i=1}^2 b_i e^{-jr\Psi_{xi}}, \quad (20)$$

$$w_{(2,r)} = \sum_{i=1}^2 c_i e^{-j\Psi_{xi}} e^{-jr\Psi_{yi}} \quad r \in \{0, 1\}. \quad (21)$$

3.2 HBF based on the linear constrained minimization of power

Though simple and straightforward, the MD BF does not take into account the power consumption in HBF design. A widely used approach for power minimization is the linear constrained minimum power (LCMP) method Trees (2002). To minimize the power consumption of BF and, in the mean time, null the interference in the beam direction of the user of interest, we apply the LCMP subject to (*s.t.*) constraints similar to that of the MD BF in (19).

Let $u_i(t), i \in \{1, 2\}$ be the transmitted signal of user i , with $E[|u_i(t)|^2] = 1$. The baseband transmitted signal for the two-user SDMA can be modeled as

$$\mathbf{x}(t) = \mathbf{s}_1 u_1(t) + \mathbf{s}_2 u_2(t). \quad (22)$$

where the steering vectors \mathbf{s}_1 and \mathbf{s}_2 are defined in (15) and (16), respectively. To design the BF weight vector \mathbf{w}_i for user i such that the output power and the interference to the beam direction of the other user are both minimized, the LCMP is formulated as

$$\arg \min_{\mathbf{w}_i} \mathbf{w}_i^H \mathbf{S}_x \mathbf{w}_i \quad (23)$$

$$\text{s.t. } \mathbf{w}_i^H \mathbf{C} = \mathbf{e}_i \quad (24)$$

where $\mathbf{S}_x \triangleq E\{\mathbf{x}^2(t)\}$, $\mathbf{C} \triangleq [\mathbf{s}_i(\phi_1, \theta_1), \mathbf{s}_i(\phi_2, \theta_2)]$ with $\{\phi_i, \theta_i\}$ being the desired beam direction of user i , and \mathbf{e}_i is a 1×2 basis vector with 1 in the i th position and the others zero.

The above optimization problem can be easily solved by making use of the Lagrange multiplier as below

$$J = \mathbf{w}_i^H \mathbf{S}_x \mathbf{w}_i + [\mathbf{w}_i^H \mathbf{C} - \mathbf{e}_i^H] \lambda + \lambda^H [\mathbf{C}^H \mathbf{w}_i - \mathbf{e}_i] \quad (25)$$

with the Lagrange multiplier $\lambda \triangleq [\lambda_1, \lambda_2]^T$. Taking the complex gradient of J respect to \mathbf{w}_i^H and setting it to zero yields

$$\mathbf{S}_x \mathbf{w} + \mathbf{C} \lambda = 0 \implies \mathbf{w} = -\mathbf{S}_x^{-1} \mathbf{C} \lambda. \quad (26)$$

Substituting (26) into (24) gives

$$-\lambda^H \mathbf{C}^H \mathbf{S}_x^{-1} \mathbf{C} = \mathbf{e}_i^H \implies \lambda^H = -\mathbf{e}_i^H [\mathbf{C}^H \mathbf{S}_x^{-1} \mathbf{C}]. \quad (27)$$

Furthermore, substituting (27) back into (26), the resultant optimal BF weight vector for user i is given by

$$\mathbf{w}_i^H = \mathbf{e}_i^H [\mathbf{C}^H \mathbf{S}_x^{-1} \mathbf{C}]^{-1} \mathbf{C}^H \mathbf{S}_x^{-1}. \quad (28)$$

4. Computer Simulations

We demonstrate simulation results for the HBF schemes studied in the previous section for SDMA. The transmit SNR in the following simulations is set to 30 dB for each user if no specific description.

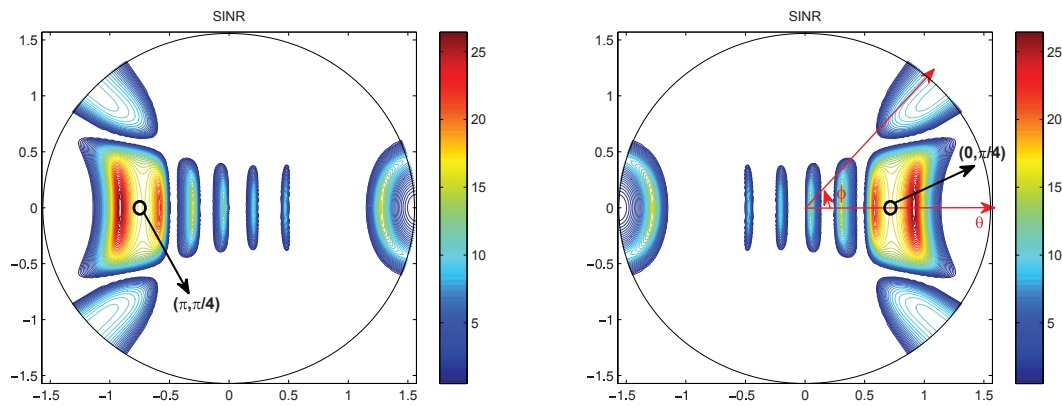


Fig. 8. The contour plots of SINR for user 1 and 2 using the RF BF. The left plot corresponds to user 2 and the right plot to user 1, with the desired directions of user one and two set at $(\phi_1, \theta_1) = (0, \pi/4)$ and $(\phi_2, \theta_2) = (\pi, \pi/4)$, respectively.

Fig. 8 presents the contour plots of the SINRs of user one and two when using the RF BF method of (4). The contour plots are shown in the cylindrical coordinate. The radial coordinate maps to the elevation angle θ and the angular coordinate maps to the azimuth angle ϕ . The desired directions of user one and two are set at $(\phi_1, \theta_1) = (0, \pi/4)$ and $(\phi_2, \theta_2) = (\pi, \pi/4)$, respectively. The resultant SINR in the desired direction of each user is equal to 16.18dB.

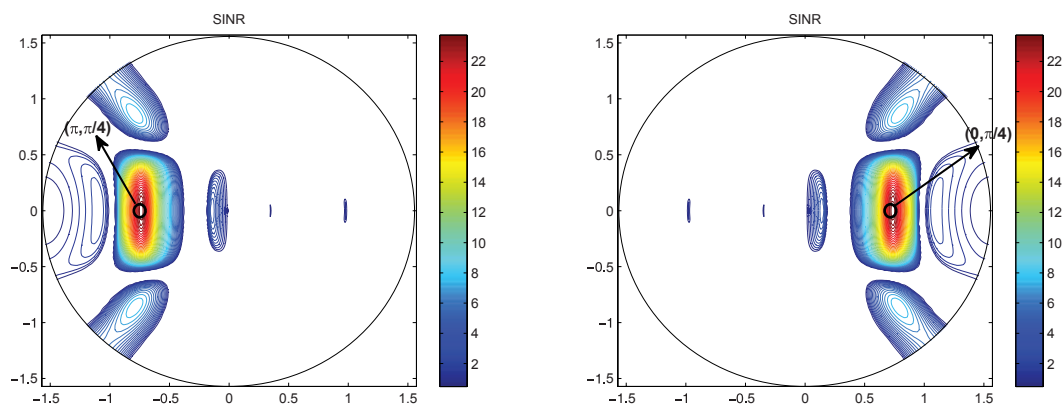


Fig. 9. The contour plots of SINR for user 1 and 2 using the HBF of LCMP. The left plot corresponds to user 2 and the right plot to user 1, with the desired directions of user one and two set at $(\phi_1, \theta_1) = (0, \pi/4)$ and $(\phi_2, \theta_2) = (\pi, \pi/4)$, respectively.

With the same simulation setting for RF BF, the contour plots of SINRs with HBF of LCMP are shown in Fig. 9. In comparison with the results in Fig. 8, we can see that the main beam here for each user is much more stronger and narrower, while the side beams are relative fewer and weaker. In addition, the resultant SINR in the desired direction of each user is now increased

to 24.09dB in Fig. 9 as oppose to the 16.18dB in Fig. 8 for the RF BF. This demonstrates that the interference can be suppressed effectively in the desired directions of users with the HBF of LCMP method. Besides, the results of HBF with MD BF are also similar to those of LCMP and, hence, are not shown here.

In addition to SINR, directivity is also an important performance measure to characterize the effectiveness of BF. To reflect the interference due to the multiple access in SDMA, the original definition for directivity in Balanis (1997) is modified into

$$D_i = \frac{4\pi \text{SINR}_i(\phi_i, \theta_i)}{\int_0^{2\pi} \int_0^{\frac{\pi}{2}} \text{SINR}_i(\phi, \theta) \sin(\theta) d\theta d\phi}. \quad (29)$$

This new definition for directivity automatically refers to the traditional notion of directivity in the single-user system.

According to this definition of directivity, Table 1 summarizes the results of SINRs, directivities and radiation powers for the RF BF and HBF schemes of MD and LCMP, respectively, when the desired directions of users are set at $(\phi_1, \theta_1) = (0, \pi/4)$ and $(\phi_2, \theta_2) = (\pi, \pi/4)$. The radiation power for each user is evaluated with

$$\int_0^{2\pi} \int_0^{\frac{\pi}{2}} |H_i(\phi, \theta)|^2 \sin(\theta) d\theta d\phi \quad (30)$$

and is denoted by P_T in the table.

It is clear from the table that HBF not only achieves higher SINRs and directivities in this case, but also uses less power for BF. This demonstrates its great potential for SDMA in mmWave applications.

User1 User2 (ϕ, θ)	User1 (0, $\pi/4$)			User2 ($\pi, \pi/4$)		
	RF	MD	LCMP	RF	MD	LCMP
SINR (dB)	16.18	24.09	24.09	16.18	24.09	24.09
Directivity	13.33	156.3	156.3	13.55	159.4	159.4
P_T	0.1388	0.0775	0.0775	0.1358	0.0764	0.0764

Table 1. The SINRs, directivities and the radiation power of the RF BF and the HBF schemes of MD and LCMP.

In addition to typical measures for the evaluation of a BF scheme, we also investigate the effectiveness of HBF from the perspective of wireless communications systems. To this end, we study the performance of a two-user SDMA with PAA in orthogonal frequency division multiplexing (OFDM) wireless communications systems. The OFDM system simulates the physical layer proposal of IEEE802.11 task group AD for very high throughput in 60GHz Channel Models for 60 GHz WLAN Systems (n.d.). Specifically, we consider an indoor simulation setting as shown in Fig. 10 for a two-user SDMA system operating in the 60GHz wireless channel model proposed for IEEE802.11ad Channel Models for 60 GHz WLAN Systems (n.d.). The system bandwidth is assumed to be 1GHz and the length of fast fourier transform (FFT) is 1024.

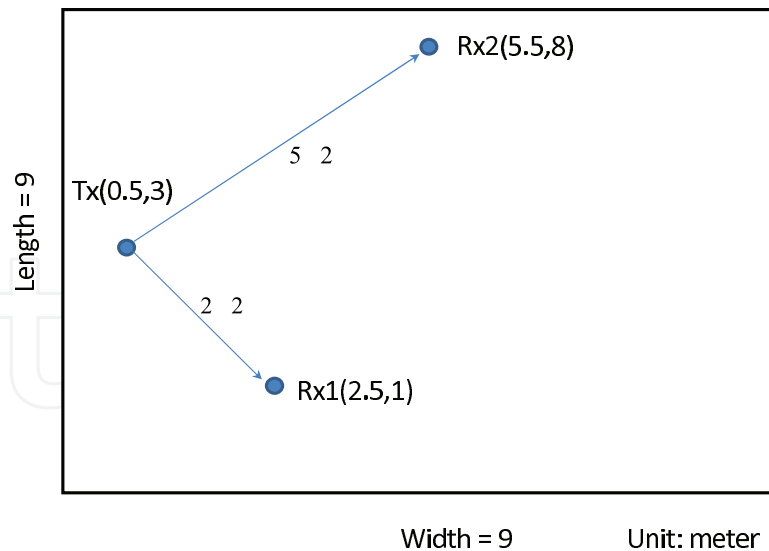


Fig. 10. The indoor simulation setting for a two-user SDMA system.

The simulated transmitter is placed at the position of (0.5, 3) from the lower left corner of the room and transmits signals simultaneously to the two users locating at (2.5, 1) and (5.5, 8), respectively, using either the RF BF setting shown in Fig. 8 or the HBF setting of LCMP in Fig. 9. The users' data are first modulated with QPSK and then transformed with the 1024-point inverse fast fourier transform (IFFT). The transformed OFDM symbol is added with a cyclic prefix of 1/8 of the OFDM symbol and then transmitted with the corresponding BF techniques to the intended users simultaneously. The transmitted signals propagate through the 60GHz channel modeled according to Channel Models for 60 GHz WLAN Systems (n.d.) to come to the two receivers of Fig. 10. At the receivers, we assume that the same RF BF with a 8×4 PAA is used by each receiver to enhance the signal qualities, supposing that the beam pattern of each user is pointed to its desired angle of arrival.

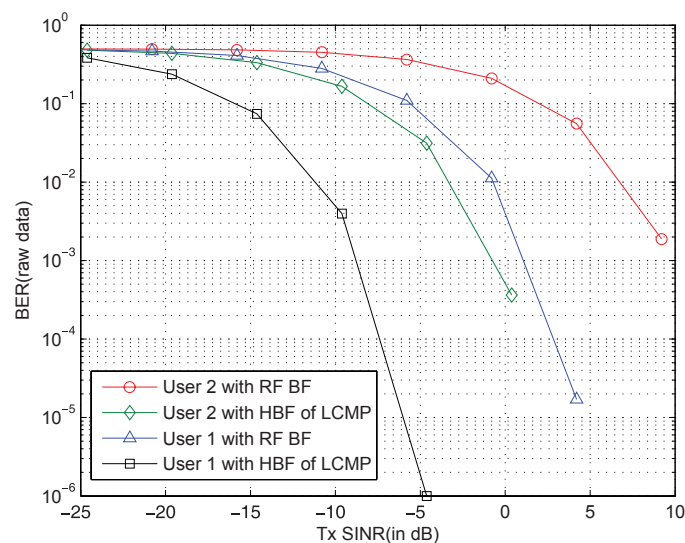


Fig. 11. The BERs for a two-user SDMA system in an indoor environment of Fig. 10.

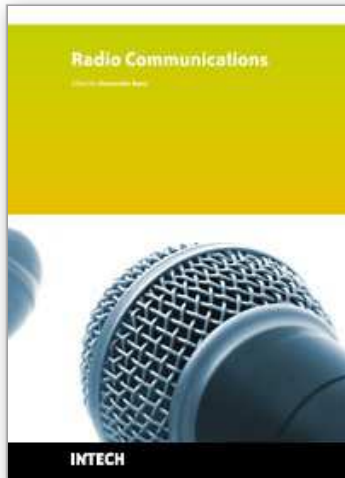
To recover the data, the receivers first remove the cyclic prefixes of each and then perform FFT followed by channel equalization for symbol detection. The bit error rate (BER) for each user is shown in Fig. 11 with respect to the transmitted SINR. As can be seen from the figure, the SNR advantages for users using the HBF of LCMP are around 10dB against the users using the RF BF only, even though the HBF gain of LCMP is only 7.91dB higher than that of RF BF.

5. Conclusions

We presented HBF techniques for SDMA in 60GHz radio using reconfigurable PAA. According to our simulation studies, the BF gain of HBF can be as much as 7.9dB higher than that of RF BF. Furthermore, the BER of using HBF in a simulated OFDM environment can have an even higher SNR advantage of 10dB against that of using the RF BF only. These results demonstrate the potential of HBF with PAA for SDMA in mmWave applications.

6. References

- Alliance, W. (n.d.). <http://www.wimedia.org/>.
- Anderson, C. R. & Rappaport, T. S. (2004). In-building wideband partition loss measurements at 2.5 and 60 GHz, *IEEE Trans. on Communications* 3(3): 922–928.
- Balanis, C. A. (1997). *Antenna Theory*, 2 edn, John Wiley & Sons.
- Balanis, C. A. & Ioannides, P. I. (2007). *Introduction to Smart Antennas*, Morgan and Claypool.
- Celik, N., Kim, W., Demirkol, M., Iskander, M. & Emrick, R. (2006). Implementation and experimental verification of hybrid smart-antenna beamforming algorithm, *IEEE Antennas and Wireless Propagation Letters* 5: 280–283.
- Channel Models for 60 GHz WLAN Systems (n.d.). 11-09-0334-02-00ad-channel-models-for-60-ghz-wlan-systems.doc. available at http://www.ieee802.org/11/Reports/tgad_update.htm.
- FCC (2004). Code of federal regulation, title 47 telecommunication, chapter 1, part 15.255.
- IEEE 802.11 WLAN Very High Throughput in 60GHz (n.d.). available at <http://www.ieee802.org/11/>.
- IEEE 802.15 WPAN Millimeter Wave Alternative PHY Task Group (TG3c) (n.d.). available at <http://www.ieee802.org/15/pub/TG3c.html>.
- Kuhwald, T. & Boche, H. (1999). A constrained beam forming algorithm for 2D planar antenna arrays, *Proc. IEEE VTC-Fall*, Amsterdam, The Netherlands.
- Rezk, M., Kim, W., Yun, Z. & Iskander, M. (2005). Performance comparison of a novel hybrid smart antenna system versus the fully adaptive and switched beam antenna arrays, *IEEE Antennas and Wireless Propagation Letters* 4: 285–288.
- Smolders, A. B. & Kant, G. W. (2000). THousand Element Array (THEA), *Proc. IEEE Antennas and Propagation Society International Symposium*, Salt Lake City, UT.
- Smulders, P. (1995). Broadband wireless LANs: a feasibility study, *Ph. D. thesis*, Eindhoven, Univ. of Tech., The Netherlands, ISBN 90-386-0100-X. available at <http://alexandria.tue.nl/extra3/proefschrift/PRF11B/9505571.pdf>.
- Smulders, P. (2002). Exploiting the 60 GHz band for local wireless multimedia access: prospects and future directions, *IEEE Communications Magazine* 2(1): 140–147.
- Trees, H. L. V. (2002). *Optimum array processing. Part. IV of detection, estimation and modulation theory.*, John Wiley & Sons.
- WirelessHD (n.d.). <http://www.wirelesshd.org/index.html>.
- Zhang, Z., Iskander, M., Yun, Z. & Host-Madsen, A. (2003). Hybrid smart antenna system using directional elements - performance analysis in flat Rayleigh fading, *IEEE Trans. on Antennas and Propagation* 51(10): 2926–2935.



Radio Communications

Edited by Alessandro Bazzi

ISBN 978-953-307-091-9

Hard cover, 712 pages

Publisher InTech

Published online 01, April, 2010

Published in print edition April, 2010

In the last decades the restless evolution of information and communication technologies (ICT) brought to a deep transformation of our habits. The growth of the Internet and the advances in hardware and software implementations modified our way to communicate and to share information. In this book, an overview of the major issues faced today by researchers in the field of radio communications is given through 35 high quality chapters written by specialists working in universities and research centers all over the world. Various aspects will be deeply discussed: channel modeling, beamforming, multiple antennas, cooperative networks, opportunistic scheduling, advanced admission control, handover management, systems performance assessment, routing issues in mobility conditions, localization, web security. Advanced techniques for the radio resource management will be discussed both in single and multiple radio technologies; either in infrastructure, mesh or ad hoc networks.

How to reference

In order to correctly reference this scholarly work, feel free to copy and paste the following:

Sau-HsuanWu, Lin-Kai Chiu, Ko-Yen Lin and Ming-Chen Chiang (2010). Planar Antenna Array Hybrid Beamforming for SDMA in Millimeter Wave WPAN, Radio Communications, Alessandro Bazzi (Ed.), ISBN: 978-953-307-091-9, InTech, Available from: <http://www.intechopen.com/books/radio-communications/planar-antenna-array-hybrid-beamforming-for-sdma-in-millimeter-wave-wpan>

INTECH
open science | open minds

InTech Europe

University Campus STeP Ri
Slavka Krautzeka 83/A
51000 Rijeka, Croatia
Phone: +385 (51) 770 447
Fax: +385 (51) 686 166
www.intechopen.com

InTech China

Unit 405, Office Block, Hotel Equatorial Shanghai
No.65, Yan An Road (West), Shanghai, 200040, China
中国上海市延安西路65号上海国际贵都大饭店办公楼405单元
Phone: +86-21-62489820
Fax: +86-21-62489821

© 2010 The Author(s). Licensee IntechOpen. This chapter is distributed under the terms of the [Creative Commons Attribution-NonCommercial-ShareAlike-3.0 License](#), which permits use, distribution and reproduction for non-commercial purposes, provided the original is properly cited and derivative works building on this content are distributed under the same license.

IntechOpen

IntechOpen